How to take into account local concentration in Ising-based Monte-Carlo: illustration with zirconium hydrides

Paul Eyméoud, Fabienne Ribeiro, Rémy Besson, Guy Tréglia

Graphical Abstract

How to take into account local concentration in Ising-based Monte-Carlo: illustration with zirconium hydrides

Paul Eyméoud,Fabienne Ribeiro,Rémy Besson,Guy Tréglia

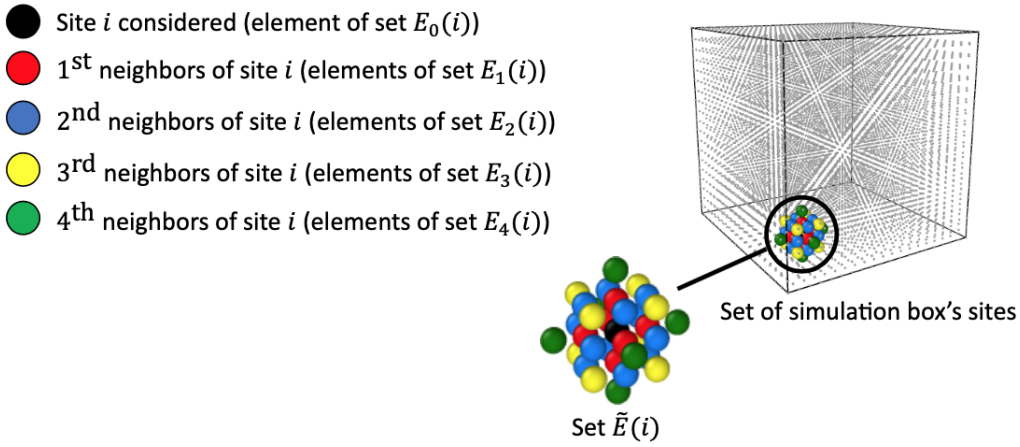

Highlights

How to take into account local concentration in Ising-based Monte-Carlo: illustration with zirconium hydrides

Paul Eyméoud,Fabienne Ribeiro,Rémy Besson,Guy Tréglia

- We develop a methodology for taking into account local atomic concentration in Ising-based Monte-Carlo bulk studies, in the specific case of intermetallics.
- Zirconium hydride studied by Monte-Carlo based on Tight-Binding Ising Model serves as a support for this study.

How to take into account local concentration in Ising-based Monte-Carlo: illustration with zirconium hydrides

Paul Eyméoud[a,*], Fabienne Ribeiro[b], Rémy Besson[c] and Guy Tréglia[d]

[a]Aix-Marseille Univ, CNRS, IM2NP Marseille, France
[b]Institut de Radioprotection et de Sûreté Nucléaire, PSN-RES, SEMIA, LSMA, 13115 St Paul Lez Durance cedex, France
[c]Univ. Lille, CNRS, INRAE, Centrale Lille, UMR 8207 - UMET - Unité Matériaux et Transformations, F-59000 Lille, France
[d]Aix Marseille Université, CNRS, CINAM, Marseille, France

ARTICLE INFO

Keywords:
Concentration-dependent Monte-Carlo
Tight-Binding Ising Model
Zirconium hydrides

ABSTRACT

We present a detailed methodology for treating local concentration dependency of pairwise interactions in Ising-based Monte-Carlo. The procedure is described through the example of interstitial ordering processes in zirconium hydrides, studied by canonical Monte-Carlo based on a concentration-dependent Tight-Binding Ising Model. The path leads to build a phase diagram of hydrogen-vacancy ordering on interstitial tetrahedral sublattice of face-centered cubic Zr-H.

1. Introduction

Many interatomic energetic models such as Embedded-Atom Method [1, 2] (EAM), Cluster Expansion Model [3] (CEM), or its simpler so-called Ising form [4], generally depend on the concentration of atomic species in the considered alloy or intermetallic. When that kind of concentration-dependent interatomic potential is used to implement a Monte-Carlo (MC) scheme, one can choose from two possible representations: (i) for all sites of the simulation box, affect the same concentration, computed by averaging compositions on the whole simulation box (the global concentration approach), (ii) for each atomic site of the simulation box, affect a specific local concentration, depending the atomic neighboring of this site (the local concentration approach).

When interatomic potentials are slowly varying with concentration, the global concentration approach (i), simpler, is generally sufficient to reproduce the correct physics for the considered system [5, 6, 7, 8]. However, in many situations, the concentration dependency of interatomic potential can be quite important. In that case, the local concentration (ii) is often required to correctly reproduce the physical behavior of the considered system. For instance, Shmakov et al. [9] have shown that the correct description of Fe-Cu alloys decomposition kinetics in CEM-based Monte-Carlo requires to take into account local concentration dependency of interactions. Similarly, Levesque et al. [10] (resp. Stukowski, Caro et al. [11, 12]) had to develop a local-concentration dependent pairwise interaction model (resp. EAM) implementing their Monte-Carlo approach, in order to correctly reproduce order *vs* segregation tendency and short-range order parameter trend with increasing at%Cr.

This question of taking or not local concentration dependency to reproduce the correct thermodynamics, is all the more important that in the case of Ising models, concentration dependency of pairwise interactions can sometimes be quite strong, with sign changes [13]. Furthermore, using clustering developments Gonis et al. [14] have demonstrated that concentration-independent interactions are rigorously valid only for strictly finite systems, such as a nanoparticle, whereas treatment of infinite systems, such as bulk alloys, requires an explicit concentration dependency of interactions. In the continuity of previously developed local concentration methodologies for interatomic potential MC studies of substitutional binary alloys [9, 10, 15], we propose here a detailed local concentration methodology for Ising-based MC studies of intermetallics. The procedure will be developed through the example of zirconium hydrides interstitial ordering, studied by a Tight-Binding Ising Model [16] (TBIM).

This article is organized as follows. First, we will briefly present the system chosen as a support for our study, namely zirconium hydrides, and the energetic model used for implementing our thermostatistical approach, TBIM. We will show the necessity, for this particular intermetallic system treated with this specific energetic model, of introducing the local concentration dependency of pairwise interactions in canonical Monte-Carlo Metropolis algorithm [17, 18], in order to correctly reproduce the ordering tendencies. This will lead us to develop a methodology for the consideration of local concentration in Monte-Carlo, and we will apply it to the construction of a phase diagram of hydrogen-vacancy ordering on interstitial tetrahedral sublattice of face-centered cubic Zr-H.

At that point, we can notice that detailed derivation of the Zr-H TBIM (recalled in section 2.2), and a preliminary Monte-Carlo study, have been already performed in Ref. [19]. However, the present investigation is clearly distinct from this previous work. In ref. [19], we failed at directly implementing the concentration-dependent TBIM in our MC with the global concentration approach, because of unphysical demixing phenomena. To overcome the problem, we implemented our global concentration approach MC with an alternative Ising model, fitted on DFT calculations by Connolly-

*Corresponding author.
paul.eymeoud@univ-amu.fr (P. Eyméoud)
ORCID(s): 0000-0003-4705-4244 (P. Eyméoud); 0000-0001-6492-2678 (F. Ribeiro); 0000-0002-5270-8698 (R. Besson); 0000-0001-9469-3140 (G. Tréglia)

Type	Stoichiometry [21]	Bravais type for Zr cage-lattice [23]	H occupancy of tetrahedral interstitial sites
γ	$ZrH_{1.0}$	FCT	H atoms located on (110) planes [23, 24]
δ	$ZrH_{1.4-1.66}$	FCC	H atoms with no particular order [24, 25, 26], potentially forming ordered patterns at low temperature [27, 28]
ε	$ZrH_{1.66-2.0}$	FCT	H atoms nearly saturating tetrahedral sites [23]

Table 1
Structural characteristics of the three main zirconium hydrides.

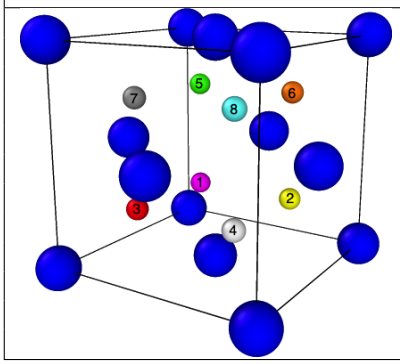

X_c	p_1^H	p_2^H	p_3^H	p_4^H	p_5^H	p_6^H	p_7^H	p_8^H
$A_{0.5}$	1	1	0	0	0	0	0	0
$B_{0.5}$	1	0	0	1	0	0	0	0
$C_{0.5}$	1	0	0	0	0	0	0	1
$A_{1.0}$	1	1	1	1	0	0	0	0
$B_{1.0}$	1	1	1	0	1	0	0	0
$C_{1.0}$	1	1	1	0	0	1	0	0
$D_{1.0}$	1	0	0	1	1	0	0	1
$E_{1.0}$	1	1	1	0	0	0	0	1
$F_{1.0}$	1	0	0	1	0	1	1	0
$A_{1.5}$	0	0	1	1	1	1	1	1
$B_{1.5}$	0	1	1	0	1	1	1	1
$C_{1.5}$	0	1	1	1	1	1	1	0

Table 2
Definition of a set of X_c ordered structures with respective $ZrH_c\square_{2-c}$ stoichiometries, using occupation factors of tetrahedral interstitial sites (p_i^H equals 1 if site i is occupied by an H atom, 0 otherwise). Elementary cell drawn with Ovito [30].

Williams inversion scheme [20]. In the present work, we manage to employ our strongly concentration-dependent TBIM in MC simulations, thanks to a local concentration methodology. This local concentration MC based on TBIM allows us to build a Zr-H schematic phase diagram (section 4), similar to the one obtained on Figure 9 of ref. [19] by global concentration MC based on DFT-fitted Ising model.

2. Position of the problem for Zr-H system

2.1. System under study

We will here focus on the case of Zr-H system, an intermetallic of particular interest in nuclear safety [21, 22].

This binary system can form several kinds of sub-stoichiometric compounds, with a face-centered cubic (FCC) or tetragonal-centered cubic (FCT) zirconium lattice, and hydrogen atoms located on tetrahedral interstitial sites. Characteristics of these intermetallic hydrides are detailed in Table 1.

In our simulations, we will consider crystallographic variants with FCC Zr lattice at cell parameter fixed at 4.82Å (equilibrium parameter of fluorite-like ZrH_2 structure determined by first-principle calculation [29]), and various hydrogen concentrations and occupations. These variants of stoichiometry $ZrH_c\square_{2-c}$, where c represents the H/Zr ratio and $\square$ an empty tetrahedral interstitial site, are described on Table 2. In our approach, this $ZrH_c\square_{2-c}$ system will be treated as a three-components alloys: zirconium Zr on FCC cage-lattice, hydrogen H on tetrahedral site, and vacancy $\square$ on tetrahedral site.

2.2. Energetic model: Tight-Binding Ising Model (TBIM)

Here is a recap of procedure and results developed in Ref. [31, 19], which will be necessary for what follows.

2.2.1. *Starting point: the Tight-Binding (TB) Hamiltonian*

The starting-point Hamiltonian model is the following Tight-Binding (TB) Hamiltonian, expressed on orthogonal atomic orbital basis $\{|i,\lambda_u\rangle\}$ (i, $\lambda = s,p,d$ and $u = \mathrm{Zr}, \mathrm{H}, \square$ respectively index site, atomic orbital and atomic type) :

$$H = \sum_i \sum_u \sum_{\lambda_u} p_i^u |i,\lambda_u\rangle \epsilon_i^{\lambda_u} \langle i,\lambda_u| + \sum_{\substack{i,j \\ i\neq j}} \sum_{u,v} \sum_{\lambda_u,\lambda_v} p_i^u p_j^v |i,\lambda_u\rangle \beta_{ij}^{\lambda_u\mu_v} \langle j,\mu_v| \quad (1)$$

where $\epsilon_i^{\lambda_u}$ denotes energy level of orbital λ of u atomic type located on site i, and $\beta_{ij}^{\lambda_u\mu_v}$ hopping integrals from orbital λ of u atomic type located on site i to orbital μ of v atomic type located on site j (here, $\beta_{ij}^{\lambda_u\mu_v}$ are assumed to be vanishing if i and j are not first-neighbors). The p_i^u factor represents the atomic occupation : it equals 1 if site i is occupied by atomic type u, and zero otherwise.

This TB Hamiltonian relies on an *spd* parameterization splitting total energy into a sum of a band term (obtained by integration of density of states), and a repulsive Born-Mayer

term [29, 31] (assumed to be fixed at given hydrogen concentration and lattice geometry): $E_{\text{tot}} = E_{\text{band}} + E_{\text{rep}}$. Only the band term will be considered in what follows. Numerical values of energy levels and hopping integrals are given in Appendix A (see [29, 31] for detailed fitting procedure).

Furthermore, computing partial electronic filling on *s*, *p*, *d* orbitals, we find a good reproduction of charge transfer (see [31], Table 4.3), coherent with H - Zr electronegativity difference: partial filling at Fermi level near 1.2 (resp., lower than 4.0) for H (resp., for Zr).

2.2.2. *Derivation procedure: the Generalized Perturbation Method*

The energetic model we will use here to implement our Monte-Carlo approach is the Tight-Binding Ising Model (TBIM). Within this model, the band energy of an ordered variant X_c of Table 2 is expressed in the following way:

$$E_{\text{band}}(X_c) \quad = \quad E_{\text{band}}(\Omega_c) + E_{\text{ord}}(X_c) \tag{2}$$

The first term of right member of equation (2), $E_{\text{band}}(\Omega_c)$, represents the band energy of H/□ interstitial disordered state Ω_c. The second term, called *ordering energy*, is the little part of the energy characterizing the specific ordered state X_c, and is defined by:

$$E_{\text{ord}}(X_c) = \frac{1}{2}\sum_{i,j}\left(p_i^{\text{H}} - \langle p_i^{\text{H}}\rangle\right)\left(p_j^{\text{H}} - \langle p_j^{\text{H}}\rangle\right)V_j(c) \tag{3}$$

Within eq. (3), differences $p_i^{\text{H}} - \langle p_i^{\text{H}}\rangle$ corresponds to the concentration fluctuation on site i with respect to the disordered state, and $V_j(c)$ denotes pairwise interaction between two hydrogen j^{th} neighbors.

These effective pairwise interactions between hydrogen atoms $V_j(c)$ appearing in equation (3) are derived from TB Hamiltonian (1) using the Generalized Perturbation Method [32, 33] (GPM) based on Coherent Potential Approximation [34, 35] (CPA).

This technique falls into two parts.

First, one needs to represent the H/□ interstitial disorder on the tetrahedral sublattice for a given composition c, by resolving the following self-consistent equation (this is what we call "CPA"):

$$c \cdot \frac{\epsilon^{s_{\text{H}}} - \Sigma(E)}{1 - (\epsilon^{s_{\text{H}}} - \Sigma(E))\bar{G}(E)} - (2-c)\cdot\frac{1}{\bar{G}(E)} = 0 \tag{4}$$

where $\bar{G}(E)$ denotes the Green's function of the disordered effective medium, and Σ a complex potential representing the effective energy level of tetrahedral interstitial site.

The second step (called "GPM") consists in taking the previously computed disordered state as a reference, and computing H-H pairwise interactions by perturbative calculation through the following analytic formula [33] (for two H atoms located on sites i_1 and i_2):

$$V_j(c) \quad = \quad -\frac{2}{\pi}\text{Im}\int_{-\infty}^{E_{\text{F}}}\left[\frac{1}{\left(1-(\epsilon^{s_{\text{H}}} - \Sigma(E))\bar{G}(E)\right)\bar{G}(E)}\right]^2$$
$$\cdot\frac{1}{N_{\vec{k}}N_{\vec{k}'}}\cdot\sum_{\vec{k},\vec{k}'}\text{Tr}\Bigg(G^{\text{HH}}_{i_1i_2}(E,\vec{k})G^{\text{HH}}_{i_2i_1}(E,\vec{k}') \cdot e^{i(\vec{k}-\vec{k}')\cdot\vec{r}_{i_1i_2}}\Bigg)\cdot dE \tag{5}$$

wherein $\vec{r}_{i_1i_2}$ denotes the distance vector between i_1 and i_2 sites, $G^{\text{HH}}_{i_1i_2}(E,\vec{k})$ the projection of Green's function $\bar{G}(E)$ on sites i_1, i_2 at point $\vec{k}$ of first Brillouin zone, $N_{\vec{k}}$ the number of $\vec{k}$ points, and E_{F} the energy at Fermi level. Formula (5) can be generalized for triplets, quadruplets, *etc*, corresponding to higher order additional terms in perturbative development (3). In practice, we have proven [31, 19] that for the Zr-H system, these multiplet interactions are negligible with respect to pairwise interactions.

2.2.3. *Result: a concentration-dependent hydrogen-hydrogen pairwise interaction model*

In Ref. [19, 31], we have applied the methodology described in section 2.2.2 to compute the H-H pairwise interactions on a large range of concentration from $c = 0.0$ to $c = 2.0$ (see Table 4 in Appendix). The procedure led to three major conclusions: (i) H-H pairwise interactions are negligible beyond fourth neighbors, (ii) orders of magnitudes ($|V_3| >> |V_1|, |V_2|, |V_4|$) point out that ordering energies are mostly driven by third-neighbors H-H pairwise interactions, (iii) signs of pairwise interactions ($V_1 > 0$, $V_2 < 0$, $V_3 < 0$, $V_4 < 0$) indicate that an hydrogen atom tends to be preferentially surrounded by vacancy at first neighborhood and hydrogen at second, third and fourth neighborhood. On top of that, we have noticed that pairwise interactions were presenting a substantial dependency in hydrogen concentration.

In order to explicit this concentration dependency of pairwise interactions, we have performed here a second-order polynomial fitting on data from Table 4, leading to the following analytic expressions in meV (V_3 corresponds to an average on the two kinds of third neighborhoods):

$$\begin{aligned} V_1 &= 7.2\cdot c - 0.2 \\ V_2 &= 4.4\cdot c^2 - 15.4\cdot c - 6.1 \\ V_3 &= 4.4\cdot c^2 + 5.7\cdot c - 70.4 \\ V_4 &= 3.9\cdot c^2 + 1.5\cdot c - 16.8 \end{aligned} \tag{6}$$

Importance of correctly implementing this concentration dependency in calculations of ordering energy and canonical Monte-Carlo algorithms will be developed next.

2.3. Reproduction of ordering processes using TBIM: order, disorder, segregation

2.3.1. *Methodology: benchmark TBIM/DFT*

In order to validate the ability of the TBIM constructed in section 2 to reproduce H/□ interstitial ordering processes on tetrahedral interstitial sub-lattice, we have performed a benchmark with Density Functional Theory [36, 37] (DFT) results. This ones have been performed at fixed geometry

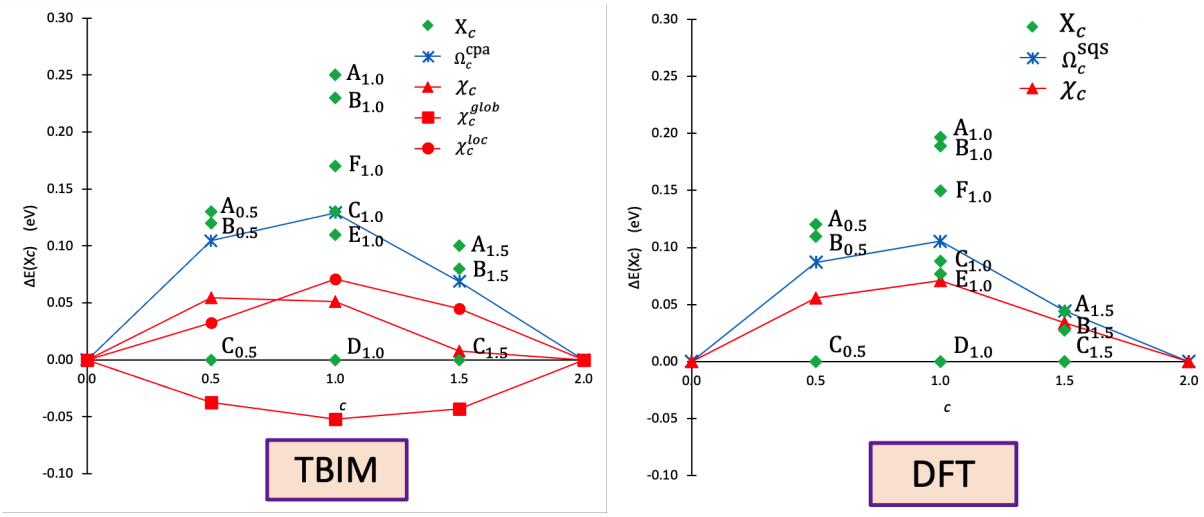

Figure 1: Sequences of formation energies with respect to the most stable ordered state (resp. Zr, $C_{0.5}$, $D_{1.0}$, $C_{1.5}$, ZrH_2 at concentrations $c = 0.0, 0.5, 1.0, 1.5, 2.0$): comparison between TBIM and DFT results. Green points correspond to ordered variants of Table 2, and blue points to the disordered state Ω_c (resp. computed using CPA/SQS technique in TBIM/DFT approach). Red triangles identify the demixed state computed using eq. (7) from Zr and ZrH_2 energies, and red squares (resp. circles) correspond to the results obtained using global (resp. local) concentration formulation of ordering energy described in section 2.3.3.

(CFC Zr cell with lattice parameter $a = 4.82$Å, fixed volume of cell, form of cell, and internal coordinates), using the Vienna Ab initio Simulation Package [38, 39], with 350 eV energy cut-off, ultrasoft pseudo-potentials [40, 41], and $13 \times 13 \times 13$ Γ-centered k-points grid. In order to represent the disordered state in DFT, we have used one 32-Zr atoms Special Quasirandom Structure [42] (SQS) per concentration, built with the *mcsqs* modulus [43] of ATAT code [44], taking into account clusters containing atomic pairs up to fourth neighboring length H-H pairs.

Energy sequences of ordered variants of Table 2, previously computed by both TBIM and DFT approach in ref. [19], are presented on Figure 1. On these graphics we have also added the novel results of disordered phase Ω_c (resp. computed using CPA/SQS technique in TBIM/DFT approach) and demixed state χ_c in order to evaluate the ordering tendency.

2.3.2. *Ability of TBIM to reproduce ordering sequences, stability of order vs disorder*

Considering Figure 1, we can draw two preliminary major conclusions. First, the procedure validates the ability of the TBIM to reproduce H/□ interstitial ordering processes, since it correctly reproduces the energy sequences of ordered variants obtained by DFT calculations (green points on graphics). Secondly, the $ZrH_c\square_{2-c}$ system tends to organize into interstitial ordered variants, rather than interstitial disorder, since for each concentration the energy of the disordered phase (blue cross on graphics) is higher than the energy of the most stable ordered variant: resp. $C_{0.5}$, $D_{1.0}$ (isomorphic to the experimentally-observed γ phase [23, 24]), $C_{1.5}$ for $c = 0.5, 1.0, 1.5$.

For $ZrH_c\square_{2-c}$, we are expecting three possible behaviors for H/□ interstitial occupation of tetrahedral sub-lattice: (i) disorder (random occupation of H), (ii) order (stability of one or several ordered variants), (iii) phase separation (segregation of H on the one hand, and □ on the other hand). We have shown the preferential stability of interstitial ordering with respect to interstitial disorder: it thus remains the question of the phase separation tendency.

2.3.3. *Stability of order vs segregation: importance of local concentration*

The energy of the demixed state χ_c at concentration c can be obtained by computing the respective energy $E(\mathrm{Zr})$ and $E(ZrH_2)$ of two independent structures Zr and ZrH_2, then applying the following formula:

$$E(\chi_c) = \frac{c}{2} \cdot E(ZrH_2) + (1 - \frac{c}{2}) \cdot E(\mathrm{Zr}) \qquad (7)$$

In DFT, terms $E(\mathrm{Zr})$ and $E(ZrH_2)$ are computed on Zr and ZrH_2 cells. In TBIM, one applies formula (7) in cases $c = 0.0$ and $c = 2.0$, wherein the ordering energy (defined by eq. (3) is vanishing, to compute $E(\mathrm{Zr})$ and $E(ZrH_2)$. Both approaches (red triangles on graphics of Fig. 1) reveal that the energy of the demixed state is higher than the one of the most stable ordered variant (resp. $C_{0.5}$, $D_{1.0}$, $C_{1.5}$ at concentrations $c = 0.5, 1.0, 1.5$). Thus, the $ZrH_c\square_{2-c}$ system tends to organize into interstitial ordered variants, rather than demix.

This energetic comparison between segregation and ordering has been based on calculations on separated Zr and ZrH_2 structures. In practice, applying a TBIM-based Monte-Carlo on a supercell, demixing phenomena will occur in the following way: a part of interstitial sites of the simulation box saturated in H, and the other part unoccupied. To compute an average ordering energy on the simulation box, two formulations are possible.

The first one, called "global concentration approach", neglects the local concentration dependency of pairwise potential. In other words, in the hydrogen-rich region (ZrH_2-like environment) of the demixed state χ_c, pairwise potential take the value $V_i(c)$. With this formulation, in eq. (3) concentration c corresponds to the ratio of number of H atoms in simulation box, on all interstitial sites of simulation box.

The second one, called "local concentration approach", takes into account local concentration dependency of pairwise potential. In other words, in the hydrogen-rich region (ZrH_2-like environment) of the demixed state χ_c, pairwise potential take the value $V_i(c = 2.0)$ (corresponding to a local environment with local concentration $c = 2.0$). With this formulation, in eq. (3) concentration c is fixed to the value $c = 2.0$ (local ZrH_2 environment).

Both approaches are numerically applied by computing ordering energy of demixed phase using eq. (3) (with c or $c = 2.0$ for global or local concentration approach), then subtracting the energy of the most stable ordered variant (resp. $C_{0.5}$, $D_{1.0}$, $C_{1.5}$ for $c = 0.5, 1.0, 1.5$). One can see that global concentration formulation of ordering energy (red squares on Fig. 1, left) leads to a unphysical segregation tendency, whereas local concentration formulation of ordering energy (red circles on Fig. 1, left) is coherent with previous results (segregation disfavored with respect to ordering).

This observation enhances the importance of taking into account local concentration in TBIM-based studies of the $ZrH_c\square_{2-c}$ system, to reproduce the ordering tendencies, which correspond to the experimental stabilities of ordered phases from Table 1. We will see in the following that this last remark, due to the substantial dependency of pairwise potentials in concentration (noticed in section 2.2.3), will take a particular importance in our Monte-Carlo study.

3. Local concentration model for Monte-Carlo

3.1. Preliminaries

We will use here a canonical Monte-Carlo Metropolis algorithm (fixed number of atoms in the simulation box). Each simulation box contains 8000 interstitial tetrahedral sites, and takes into account periodic boundary conditions. The box geometry is fixed (rigid lattice), with lattice parameter of simple cubic (SC) interstitial lattice fixed to $a/2$ with $a = 4.82$Å. For each fixed temperature, we have performed $8 \cdot 10^6$ hydrogen-vacancy exchanges in simulation box.

3.2. Insufficiency of global concentration approach in Monte-Carlo, leading to phase separation at 0K

The global concentration c in hydrogen on the simulation box, is defined as the ratio of the number of sites of the simulation box occupied by H atoms, on the total number of sites $N_{\text{box}} = 8000$ of the simulation box. It can be expressed using the following formula:

$$c = \frac{1}{N_{\text{box}}} \cdot \sum_{i=1}^{N_{\text{box}}} p_i^{\text{H}} \tag{8}$$

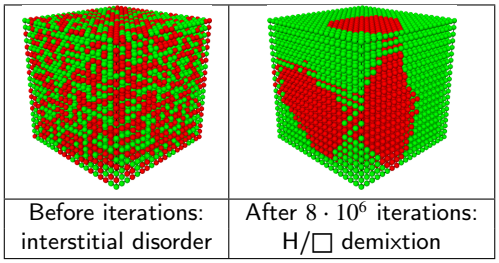

Figure 2: Global concentration approach at $c = 1.0$ and 0K: atomistic view of the simulation box (interstitial sublattice only: green for H atom, red for vacancy) before and after convergence.

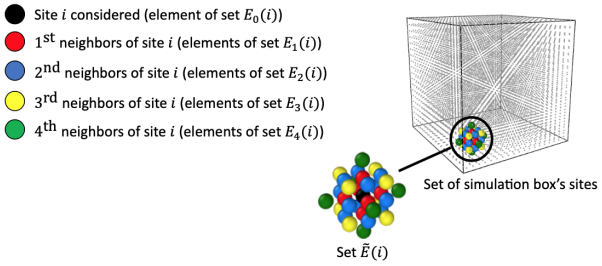

Figure 3: Schematic representation of ensemblist description used on the SC tetrahedral interstitial sublattice.

wherein p_i^{H} denotes the occupation number of interstitial site i (equals to 1 if site i is occupied by an H atom, and 0 otherwise).

In our Monte-Carlo simulations, the global concentration approach consists in assigning the value $V_i(c)$ (with c defined by eq. (8)) to a pairwise interaction V_i between two i-th neighbors of the simulation box occupied by H atoms. With this formulation, the value of pairwise interaction V_i does not depend on local hydrogen environment on the pair: for instance, a couple of two hydrogen atoms i-th neighbors will have the same value of pairwise interaction, whether it is surrounded by hydrogen (local environment ZrH_2) or vacancies (local environment Zr).

Implementation of this global concentration Monte-Carlo approach at low temperature leads to a general tendency of the system to hydrogen segregation (see Figure 2 for illustration), whatever the imposed concentration, and even though the dimensions of simulation box are increased (double dimension in each direction x,y,z). This is in contradiction with experimental observations (γ and δ stabilized phases of Table 1) and DFT results from section 2.3. Such a problem is caused by the necessity of correctly taking into account concentration dependency of pairwise potentials in order to avoid a general segregation tendency, which was previously evoked in section 2.3.3. For that reason, we will implement the local concentration dependency in Monte-Carlo, and detail the methodology.

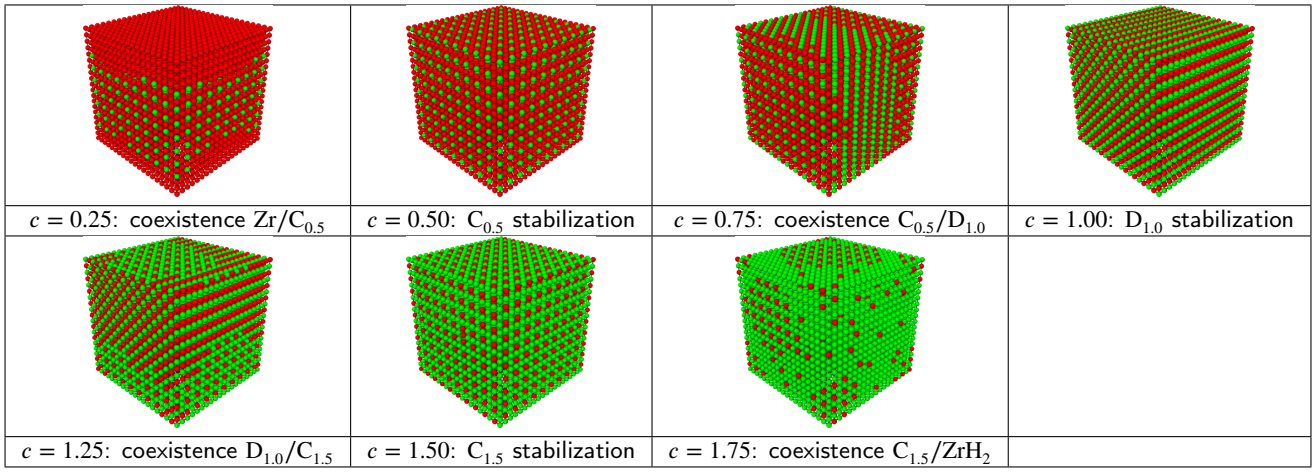

Figure 4: Simulation results at 0K with the local concentration approach: atomistic view of the simulation box (interstitial sublattice only: green for H atom, red for vacancy).

3.3. Definition of the local concentration model

In section 2.2.3, we have fitted the analytic dependency of pairwise potentials in concentration (eq. (6)).

We will now define several particular sets of interstitial sites, represented on Figure 3.

The first ones are $E_k(i)$: the site i for $k = 0$, and the sets of sites j which are k-th neighbors of i on SC interstitial sublattice for $k > 0$. Respectively, the cardinal of sets $E_0(i)$, $E_1(i)$, $E_2(i)$, $E_3(i)$, $E_4(i)$ equals to 1, 6, 12, 8, 6.

The second one is $\tilde{E}(i)$, corresponding to the union of site i and its sites first, second, third and fourth neighbors ($\mathrm{Card}(\tilde{E}(i)) = 33$):

$$\tilde{E}(i) = \bigcup_{k=0}^{4} E_k(i)$$

Considering the cluster $\tilde{E}(i)$, one can define the local concentration as the ratio between the number of sites occupied by H atoms within this cluster, on the number of total sites of this cluster:

$$c_{\mathrm{loc}}(i) = \frac{\sum\limits_{j\in\tilde{E}(i)} p_j^{\mathrm{H}}}{\mathrm{Card}(\tilde{E}(i))} = \frac{\sum\limits_{k=0}^{4}\sum\limits_{j\in E_k(i)} p_j^{\mathrm{H}}}{\sum\limits_{k=0}^{4}\mathrm{Card}(E_k(i))} \tag{9}$$

One can link local concentration (defined by eq. (9)) to global concentration (defined by eq. (8)) through the following formula, whose proof in given in Appendix C:

$$c = \frac{1}{N_{\mathrm{box}}}\cdot\sum_{i=1}^{N_{\mathrm{box}}} c_{\mathrm{loc}}(i) \tag{10}$$

Within this formalism, one can define a local ordering energy for each site i, depending on local concentration on this site:

$$E_{\mathrm{loc}}(i) = \frac{1}{2}\cdot p_i^{\mathrm{H}}\cdot\sum_{k=1}^{4}\sum_{j\in E_k(i)} p_j^{\mathrm{H}}\cdot V_j(c_{\mathrm{loc}}(i)) \tag{11}$$

The global ordering energy of the simulation box can then be expressed as the arithmetical average on all local ordering energies of the simulation box:

$$E_{\mathrm{ord}} = \frac{1}{N_{\mathrm{box}}}\cdot\sum_{i=1}^{N_{\mathrm{box}}} E_{\mathrm{loc}}(i) \tag{12}$$

3.4. Comments on the local concentration model

Equations (9), (10), (11) and (12), are defining our local concentration model.

This last one is preserving process reversibility during an occupation exchange between two sites i and j of the simulation box with different initial atomic occupations ($p_i^{\mathrm{H}} \neq p_j^{\mathrm{H}}$). In other words, if one performs the inverse exchange process (go back to initial occupation numbers), local concentrations take their values prior exchange: consequently, it will be the same for local ordering energies, and therefore for global ordering energy.

Moreover, in order to reduce CPU time, global ordering energy will be computed using formula (12) only once, before starting Metropolis algorithm. Then, at each proposition of exchange occupation between two sites i and j (with different initial occupations), we will add the energy variation ΔE with respect to initial state. This quantity ΔE will involve the sums of local ordering energies affected by the exchange, that is to say, the sum of ordering energies of sites located in neighboring environment of sites i and j:

$$\Delta E = \underbrace{\sum_{k\in\tilde{E}(i)\cup\tilde{E}(j)} E_{\mathrm{loc}}(k)}_{\text{after exchange}} - \underbrace{\sum_{k\in\tilde{E}(i)\cup\tilde{E}(j)} E_{\mathrm{loc}}(k)}_{\text{before exchange}} \tag{13}$$

3.5. Reproduction of ordering tendencies at 0K using local concentration model

Contrary to the global concentration approach used in section 3.2, which has led to a general segregation tendency, our local concentration approach defined in section 3.3 allows us to reproduce the ordering tendency at 0K. Starting

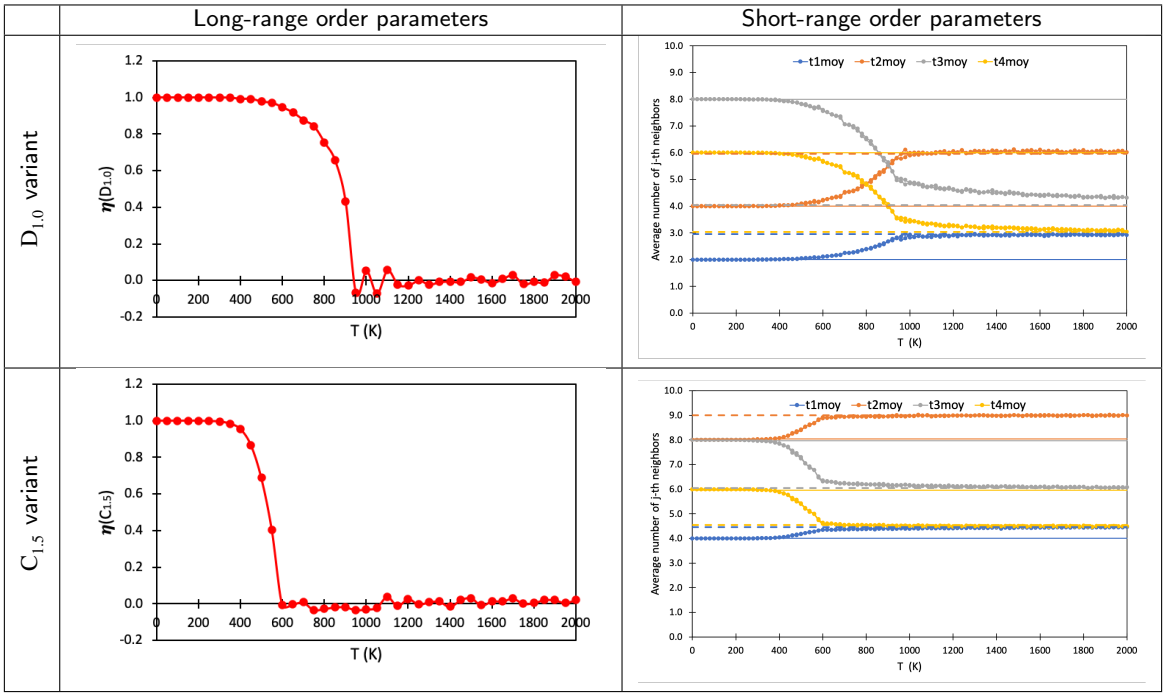

Figure 5: Order-disorder phase transition for $D_{1.0}$ and $C_{1.5}$ variants, identified by plotting long-range and short-range order parameters with respect to temperature. In short-range approach, one uses the average number of j-th H neighbors of an H atom in the simulation box, in comparison with the known values for ordered variants $t_{j\text{moy}}^{D_{1.0}}$, $t_{j\text{moy}}^{C_{1.5}}$ (continuous lines) and disordered phase $t_{j\text{moy}}^{\Omega_c} = c/2 \cdot t_{j\text{moy}}^{ZrH_2}$ (dotted lines). In long-range approach, one uses parameters defined in Appendix D (only the heating part of temperature loop is presented in this case).

from disordered state at several concentrations, we have then stabilized several characteristic ordered variants: the characteristic most-stable ordered variants $C_{0.5}$, $D_{1.0}$, $C_{1.5}$ at respective concentrations $c = 0.5, 1.0, 1.5$, and coexistence of ordered variants $Zr/C_{0.5}$, $C_{0.5}/D_{1.0}$, $D_{1.0}/C_{1.5}$, $C_{1.5}/ZrH_2$, at intermediate concentrations $c = 0.25, 0.75, 1.25, 1.75$. Atomistic views of the converged simulations are presented on Figure 4.

Moreover, at the early stages of the iterations at 0K, some twinned domains can be observed: for instance, at $c = 1.0$, germinating $D_{1.0}$ structures with different grain orientations. However, they reorganize in a single monovariant after a sufficient number of iterations ($8 \cdot 10^6$ in our approach), leading to the quasi-perfect ordered structures presented on Fig. 4.

The stable variants $D_{1.0}$, ZrH_2, $C_{1.5}$, $C_{0.5}$ can be respectively identified as γ phase (hydrogen occupation along (110) planes [23, 24], see Table 1), ε phase (H saturating tetrahedral sites [23], see Table 1), δ phase (low-temperature ordered variant with $ZrH_{1.5}$ stoichiometry [27, 28], see Table 1), ζ phase (applying an HCP from FCC structural change on this phase with Zr_2H stoichiometry [45]).

4. Application to the thermostatistical exploration of Zr-H phase diagram

We can use the local concentration model defined in section 3.3 in order to build a phase diagram of H/vacancy chemical order on interstitial tetrahedral sublattice, by canonical Monte-Carlo.

Selecting several concentrations between 0.0 and 2.0 (resp. $c = 0.25, 0.50, 0.75, 1.00, 1.25, 1.50, 1.75$), we have performed a temperature loop for each concentration, starting from a randomly-distributed H/vacancy repartition at 0K. Formation of ordered phases are identified by following the evolution of both long-range order parameters, defined in Appendix D, and Warren-Cowley short-range order parameters, defined as the average number of first, second, third and fourth hydrogen neighbors of an hydrogen atom in the simulation box $t_{j\text{moy}}$ ($j \in \{1, 2, 3, 4\}$). For instance, one can observe on Figure 5 the order-disorder phase transition (of second-order type) for $D_{1.0}$ and $C_{1.5}$ ordered variants, confirming stability of γ phase (experimentally evidenced by [46, 23, 24], see Table 1) and low-temperature interstitial ordering of δ phase (experimentally evidenced by [27, 28], see Table 1).

The path lead us to identify several cœxistence domains of ordered variants at low temperature: $Zr+C_{0.5}$, $C_{0.5}+D_{1.0}$, $D_{1.0}+C_{1.5}$, $C_{1.5}+ZrH_2$ for respective concentration ranges $c \in [0.00; 0.50], [0.50; 1.00], [1.00; 1.50], [1.50; 2.00]$. With the correspondences established in section 3.5, these domains respectively correspond to phase coexistence $Zr + \zeta$, $\zeta + \gamma$, $\gamma + \delta$, $\delta + \varepsilon$.

Such considerations are summarized on the schematic phase diagram of Figure 6. This last one is coherent with the diagram presented on Figure 9 of Ref. [19]: stabilization of $\zeta + \gamma$, $\gamma + \delta$, $\delta + \varepsilon$ domains, and order-disorder temperature

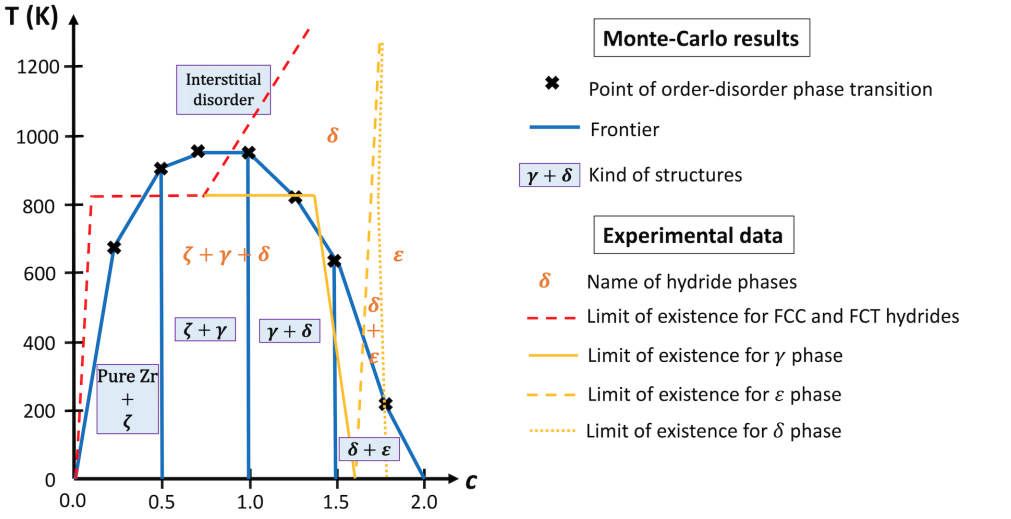

Figure 6: Phase diagram of H-vacancy interstitial ordering on the tetrahedral interstitial sublattice, resulting from our local concentration Monte-Carlo. Experimental data from [47].

respectively around 900K, 950K, and 600K for ζ, γ and δ phase.

At that time, writing [19] we were not able to use our TBIM to build the phase diagram by "classical" global concentration Monte-Carlo, since this approach was leading to a generalized hydrogen segregation tendency. To overcome this difficulty, we used an Ising model fitted on DFT calculations by Connolly-Williams inversion scheme [20].

With the new local concentration methodology presented in the present article, we have managed to correctly take into account the strong-concentration dependency of TBIM in Monte-Carlo, and stabilize, at low temperature, the same kinds of experimentally-detected ordered variants than the CEM-based global concentration Monte-Carlo of Ref. [19].

5. Conclusion and perspectives

We have first presented the system chosen as a support for our study, zirconium hydrides (section 2.1), and the energetic model chosen to implement the canonical Monte-Carlo, the Tight-Binding Ising Model (section 2.2). We have shown the importance, with those specific system and energetic model, to take into account the local concentration dependency for H-H pairwise interactions, in order to avoid a non-physical general segregation tendency (sections 2.3.3 and 3.2). We have then detailed the implementation of local concentration dependency in Monte-Carlo (sections 3.3 and 3.4). This local concentration Monte-Carlo has been then employed to build a schematic diagram of hydrogen-vacancy ordering on interstitial tetrahedral sublattice of Zr-H (section 4).

To sum up, the main interest of this work is to give a ready-to-use Monte-Carlo methodology for treating local concentration, which can be applied for any alloy or intermetallic whose ordering energy is described by an Ising model with strongly concentration-dependent pairwise interactions (which is often the case for substitutional binary alloys [13], for instance). The path can be also enlarged for more complex interatomic potentials. Particularly, several CEM [48, 49, 50], derived by Connolly-Williams inversion scheme by fits on DFT results, were developed to study interstitial ordering of zirconium hydrides by global concentration MC. It would be interesting to introduce the local concentration in these MC investigations, and evaluate its impact on phases stability.

Beyond the case of MC bulk studies of binary materials with strong concentration dependency of interatomic potentials (aforesaid intermetallic hydrides [48, 49, 50] and substitutional alloys [9, 10]), the methodology developed here can be broadened to more complex MC investigations. For instance, it can be employed to study the segregation phenomena around dislocations, implying important variations of local concentration: C around steels dislocations [51], P and Cr in α-iron dislocation core [52], *etc*. It can also be useful for investigations on high-entropy alloys, wherein local concentration fluctuations could be quite significant [53].

Acknowledgments

The authors thank ANR SIZHYP for financial support. Centre de Calcul Intensif d'Aix-Marseille is acknowledged for granting access to its high performance computing resources.

Data availability statement

The data that support the findings of this study are available from the corresponding author upon reasonable request.

Energy levels		S-K parameters		
λ_u	$\epsilon_i^{\lambda_u}$	coupling	β^0_{ZrZr}	β^0_{ZrH}
s_{H}	7.35	$dd\sigma$	-1.036	
s_{Zr}	13.0	$dd\pi$	$-0.53dd\sigma$	
p_{Zr}	18.0	$dd\delta$	$0.10dd\sigma$	
d_{Zr}	10.6	$pd\sigma$	1.179	
		$pd\pi$	$-0.30pd\sigma$	
		$pp\sigma$	2.195	
		$pp\pi$	$-0.10pp\sigma$	
		$sd\sigma$	$0.74pd\sigma$	-1.997
		$ss\sigma$	$-0.46pp\sigma$	-1.517
		$sp\sigma$	$0.66pp\sigma$	1.436

Table 3
Energy levels (in eV) and Slater-Koster parameters $\beta(r) = \beta^0_{\mathrm{ij}}\exp[-q_{ij}(r-r_{ij})/r_{ij})]$ (in eV) for hopping integrals. r_{ij} is the interatomic distance between first neighbors ($r_{\mathrm{ZrZr}} = 3.20$Å, and $r_{\mathrm{ZrH}} = 2.09$Å), $q_{\mathrm{ZrZr}} = 2.40$, and $q_{\mathrm{ZrH}} = 1.8$.

c	V_1 (meV)	V_2 (meV)	V_3 (meV)	V_4 (meV)
0.250	1.97	-9.18	-67.32	-16.41
0.500	3.46	-12.96	-67.12	-14.49
0.750	4.81	-15.67	-65.42	-13.64
1.000	6.71	-17.29	-60.97	-11.48
1.250	8.77	-18.16	-55.56	-8.68
1.500	10.77	-18.65	-50.37	-5.61
1.750	12.58	-19.12	-45.98	-2.16
2.000	14.23	-19.62	-42.74	2.03

Table 4
Pairwise interactions values between first, second, third and fourth order neighboring hydrogen atoms, with hydrogen concentration c, extracted from [31].

A. Numerical implementation of TB Hamiltonian

Table 3 gives the numerical parameters for TB Hamiltonian defined by eq. (1).

Detailed fitting procedure is given in Ref. [29, 31].

B. Data for TBIM fitting

The data employed for the fitting of formula (6) is given in Table 4.

C. Relation between global and local concentration: mathematical proof

Here, for all subset of sites A of the simulation box, the notation $\mathfrak{C}_{\mathrm{box}}(A)$ designs the complement of A in the simulation box.

Using definition (9) of local concentration, one can write:

$$\frac{1}{N_{\mathrm{box}}}\cdot\sum_{i=1}^{N_{\mathrm{box}}} c_{\mathrm{loc}}(i) = \frac{1}{N_{\mathrm{box}}}\cdot\frac{1}{33}\cdot\underbrace{\sum_{i=1}^{N_{\mathrm{box}}}\sum_{j\in\tilde{E}(i)} p_j^{\mathrm{H}}}_{=S} \tag{14}$$

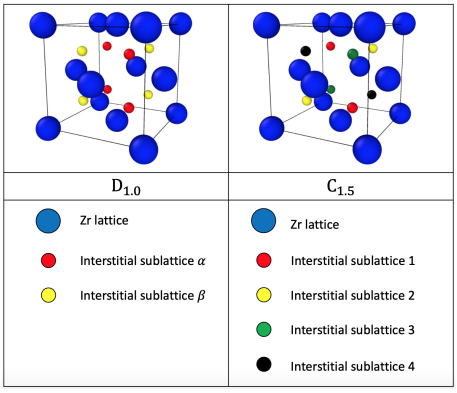

Figure 7: Representation of specific sublattices used to define long-range order parameters.

Let i a site of the simulation box, this site has 32 neighbors, which are elements of the set $\tilde{E}(i)\cap\mathfrak{C}_{\mathrm{box}}(\{i\})$.

Reciprocally, there are 32 sites l, different from i, which contain i in their set $\tilde{E}(l)$.

Therefore, among the $33\cdot N_{\mathrm{box}}$ terms of double sum S, there are 33 terms taking the value p_i^{H}.

Since this argument is valid for each sites i of the simulation box ($i\in\{1,\cdots,N_{\mathrm{box}}\}$), one can rearrange these terms to write:

$$S = \sum_{i=1}^{N_{\mathrm{box}}} 33\cdot p_i^{\mathrm{H}} \tag{15}$$

Injecting (15) in equality (14) one gets:

$$\frac{1}{N_{\mathrm{box}}}\cdot\sum_{i=1}^{N_{\mathrm{box}}} c_{\mathrm{loc}}(i) = \frac{1}{N_{\mathrm{box}}}\cdot\sum_{i=1}^{N_{\mathrm{box}}} p_i^{\mathrm{H}} \tag{16}$$

By identification with definition (8) of global concentration c, one then gets the following equation:

$$\frac{1}{N_{\mathrm{box}}}\cdot\sum_{i=1}^{N_{\mathrm{box}}} c_{\mathrm{loc}}(i) = c \tag{17}$$

corresponding to formula (10).

D. Definition of long-range order parameters

Order parameter for $\mathrm{D}_{1.0}$ (resp. $\mathrm{C}_{1.5}$) variant can be defined by dividing interstitial tetrahedral sublattice within two (resp. four) sublattices, as represented on Figure 7, then defining linear combinations of concentrations on these sublattices:

$$\begin{aligned}\eta(\mathrm{D}_{1.0}) &= c_\alpha - c_\beta\\ \eta(\mathrm{C}_{1.5}) &= \frac{1}{3}(c_2+c_3+c_4) - c_1\end{aligned}$$

As concerns $\mathrm{C}_{0.5}$ variant, one uses the definition of $\eta(\mathrm{C}_{1.5})$ with permutations $\mathrm{H}\longleftrightarrow\square$.

CRediT authorship contribution statement

Paul Eyméoud: Conceptualization, Methodology, Software, Writing - Original Draft, Writing - Review and Editing. **Fabienne Ribeiro:** Supervision. **Rémy Besson:** Software. **Guy Tréglia:** Supervision.

References

[1] M. S. Daw and M. I. Baskes, "Semiempirical, quantum mechanical calculation of hydrogen embrittlement in metals," *Physical Review Letters*, vol. 50, p. 1285, 1983. https://doi.org/10.1103/PhysRevLett.50.1285.

[2] M. S. Daw and M. I. Baskes, "Embedded-atom method: Derivation and application to impurities, surfaces, and other defects in metals," *Physical Review B*, vol. 29, p. 6443, 1984. https://doi.org/10.1103/PhysRevB.29.6443.

[3] J. M. Sanchez, F. Ducastelle, and D. Gratias, "Generalized cluster description of multicomponent systems," *Physica A: Statistical Mechanics and its Applications*, vol. 128, p. 334, 1984. https://doi.org/10.1016/0378-4371(84)90096-7.

[4] E. Ising, "Beitrag zur theorie des ferromagnetismus," *Zeitschrift für Physik*, vol. 31, p. 253, 1925. https://doi.org/10.1007/BF02980577.

[5] C. Mottet, G. Tréglia, and B. Legrand, "Theoretical investigation of chemical and morphological ordering in pdccu1-c clusters," *Physical Review B*, vol. 66, p. 045413, 2002. https://doi.org/10.1103/PhysRevB.66.045413.

[6] A. Lopes, G. Tréglia, C. Mottet, and B. Legrand, "Ordering and surface segregation in co1-cptc nanoparticles: A theoretical study from surface alloys to nanoalloys," *Physical Review B*, vol. 91, p. 035407, 2015. https://doi.org/10.1103/PhysRevB.91.035407.

[7] C. D. R. Ludwig, T. Gruhn, C. Felser, T. Schilling, J. Windeln, and P. Kratzer, "Indium-gallium segregation in cuinxga1-xse2: An ab initio–based monte carlo study," *Physical Review Letters*, vol. 105, p. 025702, 2010. https://doi.org/10.1103/PhysRevLett.105.025702.

[8] M. Y. Lavrentiev, R. Drautz, D. Nguyen-Manh, T. P. C. Klaver, and S. L. Dudarev, "Monte carlo study of thermodynamic properties and clustering in the bcc fe-cr system," *Physical Review B*, vol. 75, p. 014208, 2007. https://doi.org/10.1103/PhysRevB.75.014208.

[9] I. G. Shmakov, I. K. Razumov, O. I. Gorbatov, Y. N. Gornostyrev, and P. A. Korzhavyi, "Decomposition kinetics in fe–cu dilute alloys. monte carlo simulation using concentration-dependent interactions," *JETP Letters*, vol. 103, p. 112, 2016. https://doi.org/10.1134/S0021364016020120.

[10] M. Levesque, E. Martinez, C. C. Fu, M. Nastar, and F. Soisson, "Simple concentration-dependent pair interaction model for large-scale simulations of fe-cr alloys," *Physical Review B*, vol. 84, p. 184295, 2011. https://doi.org/10.1103/PhysRevB.84.184205.

[11] A. Stukowski, B. Sadigh, P. Erhart, and A. Caro, "Efficient implementation of the concentration-dependent embedded atom method for molecular-dynamics and monte-carlo simulations," *Modelling and Simulation in Materials Science and Engineering*, vol. 17, p. 075005, 2009. https://doi.org/10.1088/0965-0393/17/7/075005.

[12] A. Caro, D. A. Crowson, and M. Caro, "Classical many-body potential for concentrated alloys and the inversion of order in iron-chromium alloys," *Physical Review Letters*, vol. 95, p. 075702, 2005. https://doi.org/10.1103/PhysRevLett.95.075702.

[13] F. Ducastelle, "Electronic structure and ordering," *Le Journal de Physique Colloques*, vol. 38, pp. C7–272, 1977. https://doi.org/10.1051/jphyscol:1977753.

[14] A. Gonis, P. P. Singh, P. E. A. Turchi, and X. G. Zhang, "Use of the ising model in the study of substitutional alloys," *Physical Review B*, vol. 51, p. 2122, 1995. https://doi.org/10.1103/PhysRevB.51.2122.

[15] V. Pasichna and A. Gusak, "Alternative algorithms for simultaneous modeling of ordering and intermediate compound growth during reactive diffusion," *Computational Materials Science*, vol. 187, p. 110114, 2021. https://doi.org/10.1016/j.commatsci.2020.110114.

[16] G. Tréglia, B. Legrand, and F. Ducastelle, "Segregation and ordering at surfaces of transition metal alloys: the tight-binding ising model," *Europhysics Letters*, vol. 7, p. 575, 1988. https://doi.org/10.1209/0295-5075/7/7/001.

[17] N. Metropolis and S. Ulam, "The monte carlo method," *Journal of the American Statistical Association*, vol. 44, p. 335, 1949. https://www.tandfonline.com/doi/abs/10.1080/01621459.1949.10483310.

[18] N. Metropolis, A. W. Rosenbluth, M. N. Rosenbluth, and A. H. Teller, "Equation of state calculations by fast computing machines," *The Journal of Chemical Physics*, vol. 21, p. 1087, 1953. https://doi.org/10.1063/1.1699114.

[19] P. Eyméoud, F. Ribeiro, A. Charaf-Eddin, R. Besson, and G. Tréglia, "Tight-binding modeling of interstitial ordering processes in metals: Application to zirconium hydrides," *Physical Review B*, vol. 101, p. 224106, 2020. https://doi.org/10.1103/PhysRevB.101.224106.

[20] J. W. D. Connolly and A. R. Williams, "Density-functional theory applied to phase transformations in transition-metal alloys," *Physical Review B*, vol. 27, p. 5169, 1983. https://doi.org/10.1103/PhysRevB.27.5169.

[21] S. Suman, M. K. Khan, M. Pathak, R. N. Singh, and J. K. Chakravartty, "Hydrogen in zircaloy: Mechanism and its impact," *International Journal of Hydrogen Energy*, vol. 40, p. 5976, 2015. https://doi.org/10.1016/j.ijhydene.2015.03.049.

[22] A. T. Motta and L. Q. Chen, "Hydride formation in zirconium alloys," *JOM*, vol. 64, p. 1403, 2012. https://doi.org/10.1007/s11837-012-0479-x.

[23] S. S. Sidhu, N. S. S. Murthy, F. P. Campos, and D. D. Zauberis, "Neutron and x-ray diffraction studies of nonstoichiometric metal hydrides," *Advances in Chemistry*, vol. 39, p. 87, 1963. https://pubs.acs.org/doi/abs/10.1021/ba-1964-0039.ch008.

[24] A. I. Kolesnikov, A. M. Balagurov, I. O. Bashkin, A. V. Belushkin, E. G. Ponyatovsky, and M. Prager, "Neutron scattering studies of ordered gamma-zrd," *Journal of Physics: Condensed Matter*, vol. 6, p. 8977, 1994. https://doi.org/10.1088/0953-8984/6/43/004.

[25] R. C. Bowman, E. L. Venturini, and W. K. Rhim, "Proton nmr line shapes in zrhx," *Physical Review B*, vol. 26, p. 2652, 1982. https://doi.org/10.1103/PhysRevB.26.2652.

[26] V. F. Petrunin, V. P. Glazkov, V. I. Savin, V. A. Somenko, V. K. Fedotov, S. S. Shilshteyn, and S. V. Marchenko, "Investigation of phase equilibria in zirconium deuterides," *Physics of Metals and Metallography*, vol. 46, p. 181, 1978. https://pascal-francis.inist.fr/vibad/index.php?action=getRecordDetail&idt=PASCAL7940071684.

[27] L. S. Topchyan, I. A. Naskidashvili, R. A. Andrievskii, and V. I. Savin, "Low-temperature phase transitions in the zirconium-hydrogen system," *Fizika Tverdogo Tela*, vol. 15, p. 2195, 1973. https://inis.iaea.org/search/searchsinglerecord.aspx?recordsFor=SingleRecord&RN=5103417.

[28] I. N. Bydlinskaya, I. A. Naskidashvili, V. A. Melik-Shakhnazarov, and V. I. Savin, "New low-temperature phase transition in zirconium hydride," *Fizika Tverdogo Tela*, vol. 22, p. 886, 1980. https://inis.iaea.org/search/search.aspx?orig_q=RN:11569412.

[29] A. Dufresne, G. Tréglia, and F. Ribeiro, "Tight-binding n-moment potential for zirconium hydride atomistic modeling," *Metallurgical Research and Technology*, vol. 112, p. 102, 2015. https://doi.org/10.1051/metal/2014046.

[30] A. Stukowski, "Visualization and analysis of atomistic simulation data with ovito–the open visualization tool," *Modelling and Simulation in Materials Science and Engineering*, vol. 18, p. 015012, 2009. https://doi.org/10.1088/0965-0393/18/1/015012.

[31] P. Eyméoud, *Modélisation atomistique de la fragilisation des gainages combustibles nucléaires par les hydrures : caractérisation de l'ordre chimique interstitiel des hydrures de zirconium à l'aide d'un modèle d'Ising effectif dérivé des liaisons fortes*. Doctoral dissertation, Aix-Marseille Univ., 2018. http://www.theses.fr/2018AIXM0549.

[32] G. Tréglia, F. Ducastelle, and F. Gautier, "Generalised perturbation theory in disordered transition metal alloys: application to the self-consistent calculation of ordering energies," *Journal of Physics F: Metal Physics*, vol. 8, p. 1437, 1978. https://doi.org/10.1088/0305-4608/8/7/017.

[33] J. P. Landesman, G. Tréglia, P. Turchi, and F. Ducastelle, "Electronic structure and pairwise interactions in substoichiometric transition metal carbides and nitrides," *Journal de Physique*, vol. 46, p. 1001, 1985. https://doi.org/10.1051/jphys:01985004606010010O.

[34] P. Soven, "Coherent-potential model of substitutional disordered alloys," *Physical Review*, vol. 156, p. 809, 1967. https://doi.org/10.1103/PhysRev.156.809.

[35] J. S. Faulkner, "Electronic states of substoichiometric compounds and application to palladium hydride," *Physical Review B*, vol. 13, p. 2391, 1976. https://doi.org/10.1103/PhysRevB.13.2391.

[36] P. Hohenberg and W. Kohn, "Inhomogeneous electron gas," *Physical Review*, vol. 136,3B, p. B864, 1964. https://doi.org/10.1103/PhysRev.136.B864.

[37] W. Kohn and L. J. Sham, "Self-consistend equations including exchange and correlation effects," *Physical Review*, vol. 140.4A, p. A1133, 1965. https://doi.org/10.1103/PhysRev.140.A1133.

[38] G. Kresse and J. Furthmüller, "Efficiency of ab-initio total energy calculations for metals and semiconductors using a plane-wave basis set," *Comp. Mat. Sci.*, vol. 6, p. 15, 1996. https://doi.org/10.1016/0927-0256(96)00008-0.

[39] G. Kresse and J. Furthmüller, "Efficient iterative schemes for ab initio total- energy calculations using a plane-wave basis set," *Physical Review B*, vol. 54, p. 11169, 1996. https://doi.org/10.1103/PhysRevB.54.11169.

[40] D. Vanderbilt, "Soft self-consistent pseudopotentials in a generalized eigenvalue formalism," *Physical Review B*, vol. 41, p. 7892, 1990. https://doi.org/10.1103/PhysRevB.41.7892.

[41] G. Kresse and J. Hafner, "Norm-conserving and ultrasoft pseudopotentials for first-row and transition elements," *Journal of Physics: Condensed Matter*, vol. 6, p. 8245, 1994. https://doi.org/10.1088/0953-8984/6/40/015.

[42] A. Zunger, S. H. Wei, L. G. Ferreira, and J. E. Bernard, "Special quasirandom structures," *Physical Review Letters*, vol. 65, p. 353, 1990. https://doi.org/10.1103/PhysRevLett.65.353.

[43] A. Van de Walle, P. Tiwary, M. De Jong, D. L. Olmsted, M. Asta, A. Dick, D. Shin, Y. Wang, L. Q. Chen, and Z. K. Liu, "Efficient stochastic generation of special quasirandom structures," *Calphad*, vol. 42, p. 13, 2013. https://doi.org/10.1016/j.calphad.2013.06.006.

[44] A. Van de Walle, M. Asta, and G. Ceder, "The alloy theoretic automatic toolkit: A user guide," *Calphad*, vol. 26, p. 539, 2002. https://doi.org/10.1016/S0364-5916(02)80006-2.

[45] Z. Zhao, *Identification d'une nouvelle phase d'hydrure de zirconium et modélisation à l'échelle mésoscopique de sa précipitation*. Doctoral dissertation, Univ. Lille 1, 2008. https://www.theses.fr/149761805.

[46] L. Lanzani and M. Ruch, "Comments on the stability of zirconium hydride phases in zircaloy," *Journal of Nuclear Materials*, vol. 324, p. 165, 2004. https://doi.org/10.1016/j.jnucmat.2003.09.013.

[47] H. Okamoto, "H-zr (hydrogen-zirconium)," *Journal of Phase Equilibria and Diffusion*, vol. 27, p. 548, 2006. https://doi.org/10.1007/BF02736475.

[48] L. Holliger, A. Legris, and R. Besson, "Hexagonal-based ordered phases in h-zr," *Physical Review B*, vol. 80, p. 094111, 2009. https://doi.org/10.1103/PhysRevB.80.094111.

[49] L. Holliger and R. Besson, "Reciprocal-space cluster expansions for complex alloys with long-range interactions," *Physical Review B*, vol. 83, p. 174202, 2011. https://doi.org/10.1103/PhysRevB.83.174202.

[50] R. Besson and R. Candela, "Ab initio thermodynamics of fcc h-zr and formation of hydrides," *Computational Materials Science*, vol. 114, p. 254, 2016. http://dx.doi.org/10.1016/j.commatsci.2015.12.043.

[51] B. Lüthi, F. Berthier, L. Ventelon, B. Legrand, D. Rodney, and F. Willaime, "Ab initio thermodynamics of carbon segregation on dislocation cores in bcc iron," *Modelling and Simulation in Materials Science and Engineering*, vol. 27, p. 074002, 2019. https://doi.org/10.1088/1361-651X/ab28d4.

[52] I. Medouni, A. Portavoce, P. Maugis, P. Eyméoud, M. Yescas, and K. Hoummada, "Role of dislocation elastic field on impurity segregation in fe-based alloys," *Scientific Reports*, vol. 11, p. 1780, 2021. https://doi.org/10.1038/s41598-020-80140-4.

[53] S. I. Rao, C. Varvenne, C. Woodward, T. A. Parthasarathy, D. Miracle, O. N. Senkov, and W. A. Curtin, "Atomistic simulations of dislocations in a model bcc multicomponent concentrated solid solution alloy," *Acta Materialia*, vol. 125, pp. 311–320, 2017. http://dx.doi.org/10.1016/j.actamat.2016.12.011.